

Local time reversal symmetry breaking induced attenuation and localization of phonon transmission

Yu-Jia Zeng(曾育佳), Qi-Zhuang Qu(曲其壮), Zhong-Ke Ding(丁中科), and Wu-Xing Zhou(周五星)
Citation: Chin. Phys. B, 2025, 34 (**11**): 116302. DOI: 10.1088/1674-1056/adf61b
http://cpb.iphy.ac.cn; http://iopscience.iop.org/cpb

What follows is a list of articles you may be interested in

Anomalous lattice vibration in monolayer MoS_2 induced by DUV laser: A first-principles investigation

Weidong Wang(王卫东), Renhui Liu(刘仁辉), Ye Zhang(张也), Huaihong Guo(郭怀红), Jianqi Huang(黄建啟), Zhantong Liu(刘展彤), Heting Zhao(赵贺霆), Kai Wang(王凯), Bo Zhao(赵波), and Teng Yang(杨腾)
Chin. Phys. B, 2025, 34 (**6**): 066301. DOI: 10.1088/1674-1056/adc36e

Dynamic response of a thermal transistor to time-varying signals

Qinli Ruan(阮琴丽), Wenjun Liu(刘文君), and Lei Wang(王雷)
Chin. Phys. B, 2024, 33 (**5**): 056301. DOI: 10.1088/1674-1056/ad2dcc

Optical spectrum of ferrovalley materials: A case study of Janus H-VSSe

Chao-Bo Luo(罗朝波), Wen-Chao Liu(刘文超), and Xiang-Yang Peng(彭向阳)
Chin. Phys. B, 2024, 33 (**1**): 016303. DOI: 10.1088/1674-1056/acf660

Determining Hubbard *U* of VO_2 by the quasi-harmonic approximation

Longjuan Kong(孔龙娟), Yuhang Lu(陆雨航), Xinying Zhuang(庄新莹), Zhiyong Zhou(周志勇), and Zhenpeng Hu(胡振芃)
Chin. Phys. B, 2024, 33 (**1**): 016302. DOI: 10.1088/1674-1056/acfd18

Impeded thermal transport in aperiodic BN/C nanotube superlattices due to phonon Anderson localization

Luyi Sun(孙路易), Fangyuan Zhai(翟方园), Zengqiang Cao(曹增强), Xiaoyu Huang(黄晓宇), Chunsheng Guo(郭春生), Hongyan Wang(王红艳), and Yuxiang Ni(倪宇翔)
Chin. Phys. B, 2023, 32 (**5**): 056301. DOI: 10.1088/1674-1056/acb9e7

SPECIAL TOPIC — Heat conduction and its related interdisciplinary areas

Local time reversal symmetry breaking induced attenuation and localization of phonon transmission

Yu-Jia Zeng(曾育佳)[1,†], Qi-Zhuang Qu(曲其壮)[1], Zhong-Ke Ding(丁中科)[2], and Wu-Xing Zhou(周五星)[1,‡]

[1] *School of Materials Science and Engineering, Hunan University of Science and Technology, Xiangtan* 411201, *China*
[2] *School of Physics and Electronics Science, Changsha University of Science and Technology, Changsha* 410114, *China*

(Received 11 June 2025; revised manuscript received 27 July 2025; accepted manuscript online 31 July 2025)

Time-reversal symmetry (TRS) breaking induced dissipationless topological phonon edge modes provide an unprecedented way to manipulate phonon transport. However, the effect of TRS breaking on the transport properties of bulk phonon modes is still unclear. In this work, we assess the effect of local TRS-breaking domains on the transport properties of bulk phonon modes in a two-dimensional (2D) hexagonal phononic lattice model. The results show that bulk phonon modes can be strongly scattered by local TRS breaking owing to the shift of the local phonon band gap, which results in significant suppression of phonon transmission. Moreover, we show that the aperiodic distribution of local TRS-breaking domains can induce phonon Anderson localization, and the localization length can be effectively tuned by the strength of TRS breaking. Our study suggests that TRS breaking can not only be used to construct dissipationless topological phonon edge states, but also be used to block the transmission of bulk phonon modes by carefully controlling the size and distribution of TRS-breaking domains. Such results provide a highly alternative way for manipulating energy flux at the nanoscale.

Keywords: phonon transmission, time reversal symmetry, phonon localization

PACS: 63.22.–m, 63.20.D–, 66.70.–f, 61.50.Ah

DOI: 10.1088/1674-1056/adf61b **CSTR:** 32038.14.CPB.adf61b

1. Introduction

The thermal transport properties of solids and nanostructures have attracted growing interest and have promoted the fast-growing field of "phononics" owing to their important roles in thermal logic and electronic devices.[1] For instance, developing efficient thermoelectric devices requires materials with low thermal conductivity — a key challenge in the field.[2,3] Conversely, materials exhibiting high thermal conductivity are essential for addressing nanoscale heat dissipation, a major bottleneck in modern electronic devices.[4–6] So far, fruitful efforts have been devoted to manipulating phonon transport by structural modulation[7–12] or external fields.[13–15] However, new ideas and methodologies are still demanded to further manipulate phonon transport efficiently in a highly controllable and independent manner for optimizing the performance of thermoelectric, thermal management, and thermal rectification in nano-devices.

Electron topology–related physical effects, such as the quantum Hall effect, anomalous Hall effect, and spin quantum Hall effect, have revolutionized the research of condensed matter physics and materials science.[16,17] This has led to the discovery of new quantum states of matter, "topological insulators", which have been theoretically predicted and experimentally observed in various systems, including HgTe quantum wells[18] and Bi_2X_3 (X = Te, Se) crystals.[19] They are characterized by a fully insulating gap in the bulk and gapless edge or surface states that are protected by time-reversal symmetry (TRS) breaking, supporting dissipationless electronic conduction channels on the material edges, which greatly impacts the design of low-power and high-performance electronics and thermoelectrics.[20]

Phonon analogues of topological edge states are considered capable of supporting dissipationless heat-transport channels, opening up new possibilities in the field of energy transport and conversion.[21] Phonons do not couple directly with magnetic fields; thus, the TRS of vibrational states is hardly broken by external or internal magnetic fields in practical crystals. Nevertheless, several indirect approaches have been proposed to break TRS, such as the Lorentz force on charged ions and Raman spin–lattice coupling in magnetic materials.[22] Alternatively, TRS can also be theoretically broken directly by gyroscopic coupling[23] and the Coriolis force.[24,25] Inspired by these fundamental theoretical models, phonon analogues of electronic topological states have been realized in artificial metamaterials and nanomaterials, such as the kagome lattice,[26] Kekulé lattice,[27] Wigner crystal,[28] graphene-like materials,[29,30] vdW heavy fermion materials,[31] MSi (M = Fe, Mn, Co, Ni),[32] MoB_2,[33] Cu_2O,[34] and so on. Such findings pave the way for designing thermal devices based on topological phonon modes.

Crystal symmetry plays a vital role in phonon ther-

[†]Corresponding author. E-mail: zengyujia@hnust.edu.cn
[‡]Corresponding author. E-mail: wuxingzhou@hnu.edu.cn

© 2025 Chinese Physical Society and IOP Publishing Ltd. All rights, including for text and data mining, AI training, and similar technologies, are reserved.

mal conductivity and thermal rectification.[35] The crystal symmetry determines the selection rules of electron–phonon,[36,37] phonon–phonon,[38] and magnon–phonon[39,40] scattering, thus significantly influencing the thermal conductivity of materials. However, the effect of time-reversal symmetry breaking on phonon thermal transport properties has been rarely reported. Ong *et al.*[41] reported that the topological edge phonon state remains dissipationless under slight mass disorder; however, correlated disordered media can attenuate the transport of topological phonon edge states. Our previous work also shows that the robustness of topological phonon modes in crystalline materials is broken when the wave functions of two edge states overlap.[42,43] In contrast, studies on the effect of TRS breaking on the transport properties of trivial bulk phonon modes are comparatively lacking so far. In practical nanostructures, trivial bulk phonon modes are the major contributors to heat transport. Effective control of the scattering of bulk phonon modes is highly desired for thermoelectric and thermal logic devices to achieve higher performance in energy conversion and rectification. For this reason, it is necessary to understand the influence of TRS breaking on the transport of trivial bulk phonon modes.

In this work, we apply an extended atomistic Green's function method to explore the effect of local time-reversal symmetry breaking on phonon scattering and localization in a two-dimensional hexagonal phononic lattice model. We show that local TRS breaking can result in strong two-phonon scattering of bulk phonon modes, and that the scattering intensity can be tuned by the gyroscopic coupling constant. Furthermore, we show that Anderson-localized states can be formed by one-dimensionally distributed aperiodic local TRS-breaking domains. The localization length is found to be strongly modulated by the coupling constant of the TRS-breaking domains.

2. Theoretical model and methods

Here, we consider a hexagonal lattice model that is constructed from two atoms, A and B, with masses m_{A} and m_{B}, respectively. The primitive lattice is depicted in Fig. 1(a). In this model system, the phonon modes can be described by the eigenvalue equation

$$\left(\boldsymbol{H}(\boldsymbol{q}) - \omega(\boldsymbol{q})^2 \boldsymbol{M}\right) \boldsymbol{U}(q) = 0, \tag{1}$$

where $\boldsymbol{H}$ and $\boldsymbol{M}$ denote the dynamical and mass matrices, respectively. By solving this equation, the eigenvalue (frequency) $\omega(\boldsymbol{q})$ and eigenvector $\boldsymbol{U}$ of the phonon modes can be obtained. In this model, the force constants are modeled by considering the second-nearest-neighbor interactions as k_1 and $k_2 = k_1/20$. Therefore, we can define the characteristic phonon frequency as $\omega_0 = (k_1/\mu)^{1/2}$, where μ is the reduced mass of atoms A and B. According to our calculations, as the ratio k_2/k_1 increases, only the frequencies of low-energy phonons are significantly affected. On the other hand, for an actual two-dimensional material, the interaction between first-nearest neighbors is generally about one order of magnitude weaker than that between second-nearest neighbors.[44] Therefore, further increasing the ratio between k_2 and k_1 will not have any significant impact on the phonon dispersion.

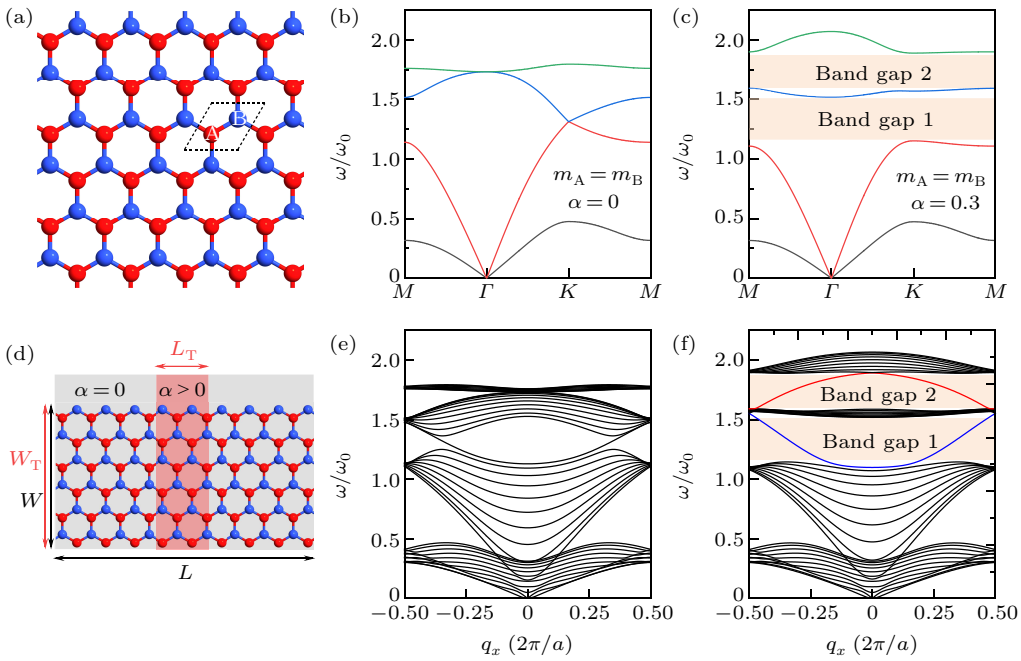


Fig. 1. (a) Schematic of the two-dimensional (2D) hexagonal phononic lattice model, showing the primitive cell surrounded by a black solid line. Bulk phonon dispersion when (b) TRS is preserved ($m_{\mathrm{A}} = m_{\mathrm{B}} = 1$) and (c) TRS is broken ($\alpha = 0.3$). (d) Schematic of the nanoribbon with total length L, width W, and the TRS-breaking domain with length L_{T} and width W_{T}. Phonon dispersion at open boundary conditions when (e) TRS is preserved ($m_{\mathrm{A}} = m_{\mathrm{B}}$ and $\alpha = 0$) and (f) TRS is broken. The gray and purple shaded areas indicate non-trivial phonon band gaps opened by TRS-breaking.

To introduce TRS breaking in this model, we adopt the gyroscopic coupling approach. For a practical nanostructure, this effect can be realized through the Lorentz force on ionic lattices or Raman spin–lattice interactions in magnetic lattices. The gyroscopic coupling simply breaks time-reversal symmetry by introducing an imaginary part into the off-diagonal elements of the mass matrix of a specific atom

$$M_{\mathrm{A(B)}} = \begin{pmatrix} m_{\mathrm{A(B)}} & \mathrm{i}\alpha \\ -\mathrm{i}\alpha & m_{\mathrm{A(B)}} \end{pmatrix}, \tag{2}$$

where α is the gyroscopic coupling constant, which is proportional to the atomic mass $m_{\mathrm{A(B)}}$. Following the above discussion, the bulk phonon dispersion at $m_{\mathrm{A}} = m_{\mathrm{B}}$ and $\alpha = 0$ is shown in Fig. 1(b), where both inversion and time-reversal symmetries are preserved. Under such conditions, we can clearly see two degenerate frequencies within the first Brillouin zone at the Γ and K points. These degenerate states can be lifted by TRS breaking, and a bulk phonon band gap (BPBG) opens when the gyroscopic coupling is nonzero, as depicted in Fig. 1(c). Such TRS-breaking-induced band gaps can support dissipationless edge phonon modes.[23]

The parameters derived from the bulk force constants can be employed to construct the tight-binding Hamiltonian under open boundary conditions. Following our previous work,[43] we apply the acoustic sum rule correction to the diagonal blocks of the Hamiltonian under open boundary conditions. The structure of the ribbon model is depicted in Fig. 1(d). We can then determine the phonon dispersion of the ribbon model both with and without gyroscopic coupling, as shown in Figs. 1(e) and 1(f). It can be clearly seen that two topological edge phonon modes appear in the two BPBGs, respectively, when TRS is broken. However, the phonon dispersion without gyroscopic coupling remains gapless. The difference in phonon dispersion reveals the mode mismatch between TRS-breaking and TRS-preserving regions, suggesting that bulk phonon modes could be blocked by TRS-breaking domains.

To calculate the phonon transmission function, we adopt the mode-resolved Green's function method. In the atomistic Green's function framework, the retarded Green's function of the central region is given by

$$\boldsymbol{G}^{\mathrm{r}}_{\mathrm{C}}(\omega) = \left(\omega^2 \boldsymbol{I}_{\mathrm{C}} - \boldsymbol{H}_{\mathrm{C}} - \boldsymbol{\Sigma}_{\mathrm{L}} - \boldsymbol{\Sigma}_{\mathrm{R}}\right)^{-1}. \tag{3}$$

The retarded surface Green's functions of the left and right leads are given by

$$\begin{aligned} \boldsymbol{g}^{\mathrm{r}}_{\mathrm{L}}(\omega) &= \left[(\omega + \mathrm{i}\eta)^2 \boldsymbol{I}_{\mathrm{L}} - \boldsymbol{H}^{00}_{\mathrm{L}} - \boldsymbol{H}^{10}_{\mathrm{L}} \boldsymbol{g}^{\mathrm{r}}_{\mathrm{L}} \boldsymbol{H}^{01}_{\mathrm{L}}\right]^{-1}, \\ \boldsymbol{g}^{\mathrm{r}}_{\mathrm{R}}(\omega) &= \left[(\omega + \mathrm{i}\eta)^2 \boldsymbol{I}_{\mathrm{R}} - \boldsymbol{H}^{00}_{\mathrm{R}} - \boldsymbol{H}^{01}_{\mathrm{R}} \boldsymbol{g}^{\mathrm{r}}_{\mathrm{R}} \boldsymbol{H}^{10}_{\mathrm{R}}\right]^{-1}, \end{aligned} \tag{4}$$

which are computed using the decimation technique. To solve for the mode-resolved phonon transmission probability, we calculate the advanced and retarded Bloch matrices of the left and right leads

$$\boldsymbol{F}^{\mathrm{a}}_{\mathrm{L}} = \boldsymbol{H}^{10}_{\mathrm{L}} \boldsymbol{g}^{\mathrm{r}}_{\mathrm{L}}, \quad \boldsymbol{F}^{\mathrm{r}}_{\mathrm{R}} = \boldsymbol{g}^{\mathrm{a}}_{\mathrm{R}} \boldsymbol{H}^{10}_{\mathrm{R}}. \tag{5}$$

The bulk eigenvector matrices $\boldsymbol{U}$ and the eigenvalue matrices corresponding to the phase factors for the leads can be determined directly from the Bloch matrices

$$\boldsymbol{F}^{\mathrm{r/a}}_{\sigma} \boldsymbol{U}^{\mathrm{r/a}}_{\sigma} = \boldsymbol{U}^{\mathrm{r/a}}_{\sigma} \boldsymbol{\Lambda}^{\mathrm{r/a}}_{\sigma}, \tag{6}$$

where $\sigma = \mathrm{L}, \mathrm{R}$, and the corresponding velocity matrices V_{σ}, needed to compute the mode-resolved phonon transmission coefficients, are defined as

$$\begin{aligned} \boldsymbol{V}_{\mathrm{L}} &= \frac{\mathrm{i}a_{\mathrm{L}}}{2\omega} \boldsymbol{U}^{\mathrm{r}}_{\mathrm{L}} \boldsymbol{H}^{10}_{\mathrm{L}} \left[\boldsymbol{g}^{\mathrm{r}}_{\mathrm{L}} - \boldsymbol{g}^{\mathrm{a}}_{\mathrm{L}}\right] \boldsymbol{H}^{01}_{\mathrm{L}} \boldsymbol{U}^{\mathrm{a}}_{\mathrm{L}}, \\ \boldsymbol{V}_{\mathrm{R}} &= \frac{\mathrm{i}a_{\mathrm{R}}}{2\omega} \boldsymbol{U}^{\mathrm{r}}_{\mathrm{R}} \boldsymbol{H}^{01}_{\mathrm{R}} \left[\boldsymbol{g}^{\mathrm{a}}_{\mathrm{R}} - \boldsymbol{g}^{\mathrm{r}}_{\mathrm{R}}\right] \boldsymbol{H}^{10}_{\mathrm{R}} \boldsymbol{U}^{\mathrm{a}}_{\mathrm{R}}. \end{aligned} \tag{7}$$

Finally, the mode-resolved phonon transmission coefficient t from the left to right lead is calculated as

$$\boldsymbol{t}_{\mathrm{LR}} = \frac{2\mathrm{i}\omega}{\sqrt{a_{\mathrm{L}} a_{\mathrm{R}}}} \boldsymbol{V}^{1/2}_{\mathrm{L}} [\boldsymbol{U}^{\mathrm{r}}_{\mathrm{L}}]^{-1} \boldsymbol{G}^{\mathrm{r}}_{\mathrm{LR}} [\boldsymbol{U}^{\mathrm{a}^{\dagger}}_{\mathrm{R}}]^{-1} \boldsymbol{V}^{1/2}_{\mathrm{R}}, \tag{8}$$

where $\boldsymbol{G}_{\mathrm{LR}}$ is given by

$$\boldsymbol{G}^{\mathrm{r}}_{\mathrm{LR}} = \boldsymbol{g}^{\mathrm{r}}_{\mathrm{L}} \boldsymbol{H}_{\mathrm{LC}} \boldsymbol{G}^{\mathrm{r}}_{\mathrm{C}} \boldsymbol{H}_{\mathrm{CR}} \boldsymbol{g}^{\mathrm{a}}_{\mathrm{R}}. \tag{9}$$

The elements of the transmission matrix $|\boldsymbol{t}|^2$ represent the transmission probability from mode i in the left lead to mode j in the right lead.

3. Results and discussion

To calculate the phonon transmission between TRS-preserving and TRS-breaking domains, we first construct a ribbon model with a sandwich structure, namely, the time-reversal symmetry of the lattice is distributed as preserving/breaking/preserving (PBP). Here, the device is divided into left (L), center (C), and right (R) parts. In the left and right leads, there is no gyroscopic coupling applied to the lattice, i.e., the strength of TRS-breaking is zero ($\alpha = 0$). In the scattering region, the TRS-breaking depends on the coupling strength α, and the shape of the TRS-breaking domain (red panel) is characterized by the number of unit cells (UC) spanning the scattering region, with length L_{T} and width W_{T}. The total length and width of the ribbon model are characterized by L and W, respectively. Therefore, we can write the device Hamiltonian as

$$\boldsymbol{H} = \begin{bmatrix} \ddots & \ddots & & & & & \\ \ddots & \boldsymbol{H}^{11}_{\mathrm{L}} & \boldsymbol{H}^{01}_{\mathrm{L}} & & & & \\ & \boldsymbol{H}^{10}_{\mathrm{L}} & \boldsymbol{H}^{00}_{\mathrm{L}} & \boldsymbol{H}_{\mathrm{LC}} & & & \\ & & \boldsymbol{H}_{\mathrm{CL}} & \boldsymbol{H}_{\mathrm{C}} & \boldsymbol{H}_{\mathrm{CR}} & & \\ & & & \boldsymbol{H}_{\mathrm{RC}} & \boldsymbol{H}^{00}_{\mathrm{R}} & \boldsymbol{H}^{01}_{\mathrm{R}} & \\ & & & & \boldsymbol{H}^{10}_{\mathrm{R}} & \boldsymbol{H}^{11}_{\mathrm{R}} & \ddots \\ & & & & & \ddots & \ddots \end{bmatrix}. \tag{10}$$

Here, we apply the extended atomistic Green's function method, originally developed by Ong *et al.*[45–47] and further extended in our previous work under open boundary conditions,[42] to calculate the phonon mode-resolved transmission probability.

Figure 2 presents the mode-resolved phonon transmission probabilities for modes with positive group velocities. When TRS is preserved throughout the entire nanoribbon, the transmission probability for each phonon mode remains strictly at 1.0, due to the perfect frequency matching between the bulk leads and the central region. In contrast, as the TRS-breaking strength α increases from 0.2 to 0.6, the phonon transmission probability exhibits a significant reduction. Notably, phonon modes near the center of the Brillouin zone with lower group velocities are more susceptible to the influence of local TRS-breaking. Additionally, a distinct cutoff frequency emerges, above which phonon transmission is strongly suppressed. This suppression arises because the corresponding propagating modes are entirely localized at the edges, as confirmed by the local density of states shown in Fig. 3(a). Such edge-dominated transport channels are supported by non-trivial local phonon band gaps within the TRS-breaking domain. Furthermore, the cutoff frequency can be tuned by adjusting the coupling strength α, since the upper and lower edges of the band gap shift with increasing α. It should be noted that we adopt a two-dimensional hexagonal lattice model in this work; thus, the transmission of out-of-plane vibrational phonon modes is ignored. Liu *et al.* pointed out that out-of-plane and in-plane vibrations are generally decoupled from each other in an atomically flat structure such as graphene. Even when they are allowed to hybridize in a buckled structure, leading to avoided crossings in the phonon dispersion, the hybridization does not break the degeneracy and thus does not alter the topological nature of phonons.[22] Therefore, we focus on discussing the transmission of in-plane vibrations.

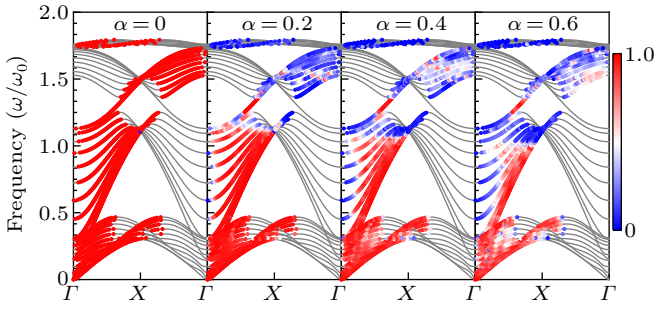


Fig. 2. Mode-resolved phonon transmission of the left lead for different coupling strengths, with a width of $W = W_T = 5$ UC. The transmission probability, ranging from 0 to 1, is indicated by color according to the side color bar.

The introduction of TRS-breaking disrupts the translational invariance of the force constant matrix along the transport direction. Consequently, well-defined dispersion relations can no longer be directly compared between the TRS-preserving ($\alpha = 0$) and TRS-breaking ($\alpha > 0$) regions. Nevertheless, it is heuristically valuable to interpret how local TRS-breaking affects the transport of bulk phonon modes. To this end, we compare the phonon density of states (PDOS) in the central region under both TRS-preserving and TRS-breaking conditions, as shown in Fig. 3(a). It can be clearly seen that local TRS-breaking induces localization of bulk phonon modes below $0.5\,\omega/\omega_0$. More notably, the PDOS above $0.8\,\omega/\omega_0$ exhibits significant changes as α increases from 0 to 0.8: the PDOS peaks shift toward lower frequencies, and the corresponding vibrational states become increasingly localized.

To quantitatively describe this behavior, we further calculate the lower and upper frequencies of two BPBGs. As shown in Fig. 3(b), the lower edge of BPBG-1 consistently shifts toward lower frequencies, while its upper edge first increases and then decreases with α. In contrast, BPBG-2 shows the opposite trend. Interestingly, the downward shift of the lower edge of BPBG-1 correlates well with the observed peak shift in the PDOS. Moreover, the frequency difference between the upper and lower edges defines the absolute band gap, which exhibits a nonmonotonic evolution: both absolute band gaps initially widen and subsequently narrow as the TRS-breaking strength α increases. A critical transition occurs around $\alpha = 0.27$.

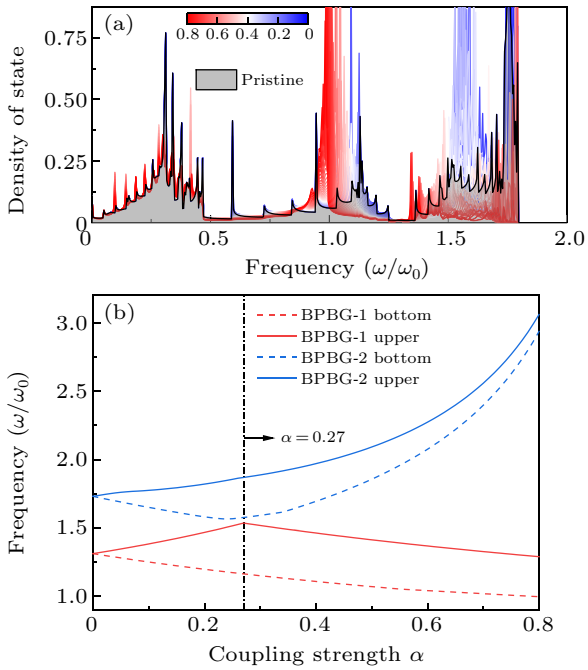


Fig. 3. (a) Phonon density of states (DOS) for a TRS-breaking domain of width $W_T = 5$ UC. Colored lines indicate the phonon DOS at different coupling strengths $\alpha \in [0, 0.8]$. (b) Frequencies at the lower and upper edges of bulk phonon band gaps 1 and 2 as a function of coupling strength α.

Based on the analysis of bulk phonon dispersion, each TRS-breaking-induced local BPBG supports only a single edge phonon branch under open boundary conditions. Therefore, the scattering of bulk phonon modes primarily arises

from variations in the local band gap. When bulk phonon states fall within the frequency range of the local band gap, transport becomes confined to a single edge phonon channel, while all other propagating modes are strongly suppressed.

To assess the influence of local TRS-breaking on phonon thermal transport, we show the contour of total phonon transmission as a function of α for different TRS-breaking domain sizes, as shown in Figs. 4(a)–4(c). The transmission of low-frequency phonon modes (below $0.5\,\omega/\omega_0$) is less affected when the width of the TRS-breaking domain is smaller than the width of the ribbon. However, it is evident that high-frequency phonon modes are significantly suppressed with increasing coupling strength and width of the TRS-breaking domain. Once localized TRS-breaking is introduced, the transmission gap between 1.25–$1.37\,\omega/\omega_0$ consistently occurs, even when the TRS-breaking domain does not span the entire width of the nanoribbon. In addition, the transmission gap initially increases and then decreases with increasing coupling strength, as shown in Fig. 4(d). This variation in the transmission gap corresponds to the shift in the phononic band gap discussed previously.

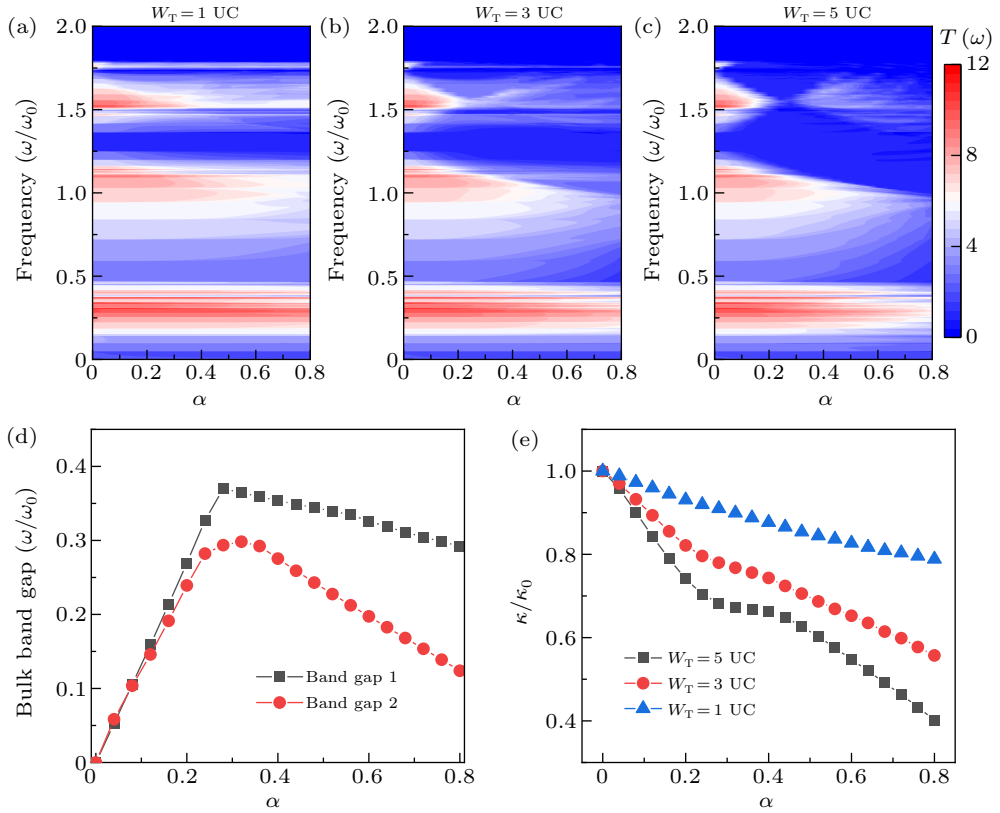


Fig. 4. Contours of the total phonon transmission function and thermal conductance as a function of gyroscopic coupling strength α for different widths: (a) $W_T = 1$ UC, (b) $W_T = 3$ UC, and (c) $W_T = 5$ UC. (d) Bulk band gaps as a function of gyroscopic coupling strength α. (e) Thermal conductance ratio κ/κ_0 as a function of α, where κ_0 is the thermal conductance for the TRS-preserving configuration.

To assess the thermal transport, we calculate the dimensionless ratio κ/κ_0 as a function of α, where κ_0 and κ are the thermal conductances of the TRS-preserved and TRS-breaking configurations, respectively. As shown in Fig. 4(e), κ/κ_0 decreases monotonically with increasing TRS-breaking strength, and this trend is strongly influenced by the width of the local TRS-breaking domain. This behavior is primarily governed by the degree of hybridization between the phonon dispersions of the TRS-breaking and TRS-preserving domains. When the TRS-breaking domain spans the full width of the nanoribbon, the change in thermal conductance becomes more gradual near the critical transition point. In this case, the local band gap is entirely determined by the coupling strength α, and bulk phonon transport channels are suppressed. However, when the TRS-breaking domain is narrower than the nanoribbon, the vibrational states in the central region arise from the hybridization between TRS-breaking and TRS-preserving domains, thereby providing additional transmission channels for bulk phonon modes.

The fundamental relationship between TRS-breaking domains and phonon transmission indicates that a local TRS-breaking domain can both scatter bulk phonon modes and support a robust edge transport channel. Theoretically, when an edge phonon mode originating from a TRS-breaking domain enters a TRS-preserving region, it transforms into a trivial bulk phonon mode. To clarify this behavior, we further examine the effect of doping on phonon transmission. For comparison, two cases are considered: in the first case, only the TRS-breaking domain is doped; in the second case, the entire nanoribbon is

uniformly doped. In both cases, the phonon transmission is averaged over more than 100 randomly generated doping configurations, with the dopant concentration fixed at 50%.

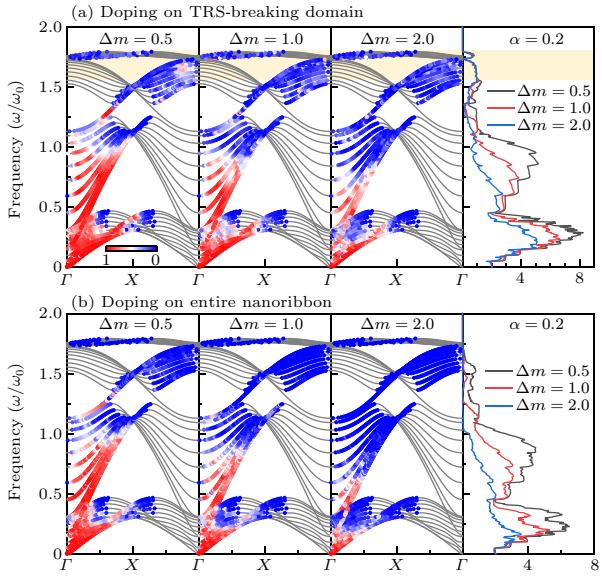


Fig. 5. Mode-resolved and total phonon transmission probabilities from the left to right lead for (a) doping within the TRS-breaking domain and (b) doping across the entire nanoribbon, under different doping strengths Δm.

The mode-resolved and total phonon transmission probabilities for the two cases are shown in Figs. 5(a) and 5(b). It can be seen that the edge-state transport channel provided by the local TRS-breaking domain can be destroyed by impurities regardless of the region in which the doping is performed. Remarkably, the total transmission of high-frequency bulk phonons remains robust even as the doping strength Δm increases from 0.5 to 2.0, provided that the doping is confined to the TRS-breaking domain, as indicated by the yellow shaded area in Fig. 5(a). On the other hand, the effect of doping on phonon modes with frequencies below $1.0\,\omega/\omega_0$ is essentially the same in both cases, with transmission probabilities decreasing monotonically with increasing doping strength (Δm). Generally, high-frequency phonon modes are more susceptible to impurities. However, the results suggest that their transmission can be preserved by introducing a local TRS-breaking domain within the doped region. The robustness of bulk phonon transport against impurity scattering primarily arises from the presence of edge channels supported by the locally TRS-breaking domain. When bulk phonons encounter these domains, their modes can be converted into topological edge phonon states, allowing them to traverse the doped region while avoiding impurity scattering. Although the phonons revert to bulk modes after exiting the TRS-breaking domain, they can still be transmitted from the left to the right lead, as long as their frequencies match those within the bulk phonon dispersion of the leads. This topological protection mechanism enables bulk phonons to bypass impurity scattering via temporary conversion into edge states within the TRS-breaking region before re-entering the bulk dispersion in the leads. Moreover, as discussed previously, the frequency range of this transport channel is tunable. Leveraging this feature, phonon transport at specific frequencies can be selectively enabled by adjusting the strength of the local TRS-breaking domain.

To further understand the effect of TRS-breaking on bulk phonon transport, we construct an aperiodic superlattice (ap-SL), as depicted in Fig. 6(a). The localization length is extracted from the exponential decay of the transmission coefficient, $\tau(\omega, q) = \tau_0(\omega, q)\exp(L/\xi)$, with respect to the central region length, providing direct evidence of phonon Anderson localization.[48,49] Here, we emphasize that the phonon transmission coefficient in the long-wavelength limit is 1.0 for different lengths, and thus their localization length should be infinite, whereas the exponential fitting yields a finite value. In previous studies, these phonon modes are categorized as ballistic modes. However, research on mass-disordered superlattices indicates that phonon Anderson localization is actually ubiquitous when the central region is sufficiently long and strongly disordered.[50–52] Therefore, the localization length of phonon modes larger than the system size is treated as a simple extrapolation value from the exponential fitting in this work. To ensure accuracy, we verified the reliability of these extrapolated values under different truncated system sizes.

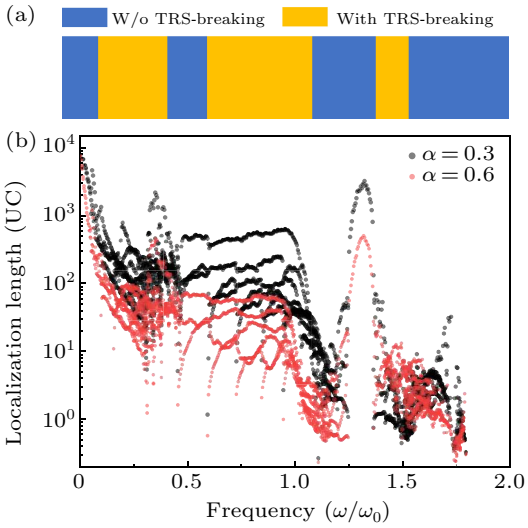


Fig. 6. (a) Schematic of an aperiodic time-reversal symmetry breaking/preserving superlattice. (b) Localization lengths of individual phonon modes in the ap-SL for coupling strengths $\alpha = 0.3$ (black dots) and $\alpha = 0.6$ (red dots).

We present the results with the truncated system size $L = 200$ UC in Fig. 6(b) (black dots) for all individual phonon modes. The results clearly show that disordered local TRS-breaking domains can also induce phonon Anderson localization. More interestingly, we investigate whether the strength of symmetry breaking can effectively tune the localization length without changing the number of interfaces. For this purpose, we calculate the localization length at $\alpha = 0.6$ with the same truncated system size (red dots in Fig. 6(b)). The localization

length of the majority of phonon modes, including topological edge modes, decreases by up to one order of magnitude with the increase of coupling strength, and their localization lengths are mostly distributed within 1–100 UC. Only the localization lengths of phonon modes in the low-frequency range are less affected by the strength of TRS-breaking. In addition, the phonon modes within the local topological band gap are also significantly influenced by the strength of TRS-breaking. These results suggest that localization lengths can be tuned by the strength of TRS-breaking.

4. Conclusion

In summary, using the mode-resolved Green's function method, we provide mode-level insight into the effect of local time-reversal symmetry breaking on phonon transport properties. Local TRS-breaking can enlarge local phonon band gaps and shift the bulk phonon dispersion, resulting in strong scattering of bulk phonons and suppression of thermal conductance. More importantly, we demonstrate that aperiodic local TRS-breaking domains can induce phonon Anderson localization, and the localization length can be tuned by adjusting the strength of TRS-breaking. Our results suggest that local time-reversal symmetry breaking can serve as an independent method to manipulate phonon transport. Given that local TRS-breaking can be realized via charged ions or spin–lattice interactions under an external magnetic field, we expect that local TRS-breaking in crystals is a promising approach for manipulating phonon transport at the nanoscale. This will promote the development of high-performance thermoelectric and thermal logical devices.

Acknowledgments

This work was supported by the National Natural Science Foundation of China (Grant No. 12404011), the Natural Science Foundation of Hunan Province (Grant No. 2023JJ40273), and the Scientific Research Foundation of Hunan Provincial Education Department (Grant No. 23B0495).

References

[1] Li N, Ren J, Wang L, Zhang G, Hänggi P and Li B 2012 *Rev. Mod. Phys.* **84** 1045
[2] Chen X K, Zhu J, Qi M, Jia P Z and Xie Z X 2025 *Phys. Rev. Appl.* **23** 034085
[3] Zheng Y H, Zeng Y J, Xie G F and Zhou W X 2024 *J. Appl. Phys.* **136** 164301
[4] Zeng Y J, Wu D, Cao X H, Zhou W X, Tang L M and Chen K Q 2020 *Adv. Funct. Mater.* **30** 1903873
[5] Gu X, Wei Y, Yin X, Li B and Yang R 2018 *Rev. Mod. Phys.* **90** 041002
[6] Chen J, Xu X F, Zhou J and Li B W 2022 *Rev. Mod. Phys.* **94** 025002
[7] Meng X, Pandey T, Jeong J, Fu S, Yang J, Chen K, Singh A, He F, Xu X and Zhou J 2019 *Phys. Rev. Lett.* **122** 155901
[8] Wu C W, Ren X, Li S Y, Zeng Y J, Zhou W X and Xie G 2022 *Appl. Phys. Lett.* **121** 172201
[9] Zeng Y J, Wu D, Cao X H, Feng Y X, Tang L M and Chen K Q 2020 *J. Mater. Chem. A* **8** 11884
[10] Zeng Y J, Feng Y X, Tang L M and Chen K Q 2021 *Appl. Phys. Lett.* **118** 183103
[11] Wei Y and He D 2023 *Chin. Phys. Lett.* **40** 090502
[12] Wu M, Shi R, Qi R, Li Y, Feng T, Liu B, Yan J, Li X, Liu Z and Wang T 2023 *Chin. Phys. Lett.* **40** 036801
[13] Jin H, Restrepo O D, Antolin N, Boona S R, Windl W, Myers R C and Heremans J P 2015 *Nat. Mater.* **14** 601
[14] Tang D S and Cao B Y 2021 *Int. J. Heat Mass Transfer* **179** 121659
[15] Sheng Y, Zhu H, Xie S, Lv Q, Xie H, Wang H, Lv R and Bao H 2025 *Nat. Commun.* **16** 1970
[16] Hasan M Z and Kane C L 2010 *Rev. Mod. Phys.* **82** 3045
[17] Qi X L and Zhang S C 2011 *Rev. Mod. Phys.* **83** 1057
[18] Bernevig B A, Hughes T L and Zhang S C 2006 *Science* **314** 1757
[19] Chen Y L, Analytis J G, Chu J H, Liu Z K, Mo S K, Qi X L, Zhang H J, Lu D H, Dai X and Fang Z 2009 *Science* **325** 178
[20] Xu Y, Gan Z X and Zhang S C 2014 *Phys. Rev. Lett.* **112** 226801
[21] Ding Z K, Zeng Y J, Liu W, Tang L M and Chen K Q 2024 *Adv. Funct. Mater.* **34** 2401684
[22] Liu Y, Xu Y, Zhang S C and Duan W 2017 *Phys. Rev. B* **96** 064106
[23] Wang P, Lu L and Bertoldi K 2015 *Phys. Rev. Lett.* **115** 104302
[24] Wang Y T, Luan P G and Zhang S 2015 *New J. Phys.* **17** 073031
[25] Kariyado T and Hatsugai Y 2015 *Sci. Rep.* **5** 18107
[26] Stenull O, Kane C L and Lubensky T C 2016 *Phys. Rev. Lett.* **117** 068001
[27] Liu Y, Lian C S, Li Y, Xu Y and Duan W 2017 *Phys. Rev. Lett.* **119** 255901
[28] Ji W C and Shi J R 2017 *Chin. Phys. Lett.* **34** 036301
[29] Tao Z, Wang Y, He S, Li J, Xue S, Su Z, Sun J, Peng H, Guo J and Zhu X 2025 *Chin. Phys. Lett.* **42** 027405
[30] Li J, Wang L, Liu J, Li R, Zhang Z and Chen X Q 2020 *Phys. Rev. B* **101** 081403
[31] Li F, Yu T, Lai J, Liu J, Liu P, Chen X Q and Sun Y 2024 *Chin. Phys. Lett.* **41** 107301
[32] Zhang T, Song Z, Alexandradinata A, Weng H, Fang C, Lu L and Fang Z 2018 *Phys. Rev. Lett.* **120** 016401
[33] Zhang T T, Miao H, Wang Q, Lin J Q, Cao Y, Fabbris G, Said A H, Liu X, Lei H C, Fang Z, Weng H M and Dean M P M 2019 *Phys. Rev. Lett.* **123** 245302
[34] Wang Z, Zhou W, Rudenko A and Yuan S 2021 *Phys. Rev. B* **103** 195137
[35] Jiang P, Hu S, Ouyang Y, Ren W, Yu C, Zhang Z and Chen J 2020 *J. Appl. Phys.* **127** 235101
[36] Alidoosti M, Esfahani D N and Asgari R 2022 *Phys. Rev. B* **106** 045301
[37] Yang Q L, Li W, Wang Z, Ning F l and Luo J W 2024 *Phys. Rev. B* **109** 125203
[38] Yang R, Yue S, Quan Y and Liao B 2021 *Phys. Rev. B* **103** 184302
[39] Pan H, Tang L M and Chen K Q 2022 *Phys. Rev. B* **105** 064401
[40] Pan H, Ding Z K, Zeng B W, Luo N N, Zeng J, Tang L M and Chen K Q 2023 *Phys. Rev. B* **107** 104303
[41] Ong Z Y and Lee C H 2016 *Phys. Rev. B* **94** 134203
[42] Ding Z K, Zeng Y J, Pan H, Luo N, Tang L M, Zeng J and Chen K Q 2024 *Phys. Rev. B* **109** 245104
[43] Ding Z K, Zeng Y J, Pan H, Luo N, Zeng J, Tang L M and Chen K Q 2022 *Phys. Rev. B* **106** L121401
[44] Zimmermann J, Pavone P and Cuniberti G 2008 *Phys. Rev. B* **78** 045410
[45] Ong Z Y and Zhang G 2015 *Phys. Rev. B* **91** 174302
[46] Ong Z Y 2018 *Phys. Rev. B* **98** 195301
[47] Ong Z Y 2018 *J. Appl. Phys.* **124** 151101
[48] Juntunen T, Vänskä O and Tittonen I 2019 *Phys. Rev. Lett.* **122** 105901
[49] Hu S, Zhang Z, Jiang P, Chen J, Volz S, Nomura M and Li B 2018 *J. Phys. Chem. Lett.* **9** 3959
[50] Hu R and Tian Z 2021 *Phys. Rev. B* **103** 045304
[51] Hu S, Zhang Z, Jiang P, Ren W, Yu C, Shiomi J and Chen J 2019 *Nanoscale* **11** 11839
[52] Sun L, Zhai F, Cao Z, Huang X, Guo C, Wang H and Ni Y 2023 *Chin. Phys. B* **32** 056301